

Optimising rPPG Signal Extraction by Exploiting Facial Surface Orientation

Kwan Long Wong^{1,2*}, Jing Wei Chin^{1,2*}, Tsz Tai Chan², Ismoil Odinaev²
Kristian Suhartono², Kang Tianqu¹, Richard H.Y. So^{1,2}

¹The Hong Kong University of Science and Technology, ²PanopticAI Ltd.

Abstract

Remote photoplethysmography (rPPG) is a contactless method to measure human vital signs by detecting subtle skin color changes through a camera. Although many studies have used region of interest (ROI) selection tools to improve rPPG signal extraction, no study has investigated the influence of the ROI's surface orientation. We propose a novel 'angle map' representation of the face to study the effects of the surface orientation on the extracted rPPG signal. The angle map is generated by mapping each facial pixel to an angle of reflection (angle between the skin surface and the camera) calculated from the surface normal of the facial landmarks and the camera axis. Our results show that surface orientation significantly affects the correlation between the extracted rPPG signal and ground truth blood volume pulse (BVP). Regions with small angles of reflection contained stronger signals, which explains why areas near the cheeks and forehead are often chosen for rPPG signal extraction. Moreover, we applied a thresholding method to the angle map and demonstrated its potential for dynamic ROI selection, thereby optimising the rPPG signal extraction process.

1. Introduction

Over the last decade, remote measurement of human vital signs has received growing attention in the research community. Remote photoplethysmography (rPPG) is an optical technique that measures physiological signals from facial videos by analysing subtle blood volume changes under the skin. From the rPPG signal, researchers have been able to extract vital signs such as heart rate [14, 25], respiration rate [19, 27], blood pressure [6, 26], and oxygen saturation [9, 21].

Due to the nature of remote measurement, the rPPG signal is susceptible to various sources of noise. Small differences in illumination [16, 17], camera specification [15, 22],

subject motion [5, 24] and distance to the camera [1, 8], skin tone [10, 18], and make-up [28] can significantly impact the quality of the extracted signal. As the signal-to-noise ratio (SNR) varies across different face areas, region of interest (ROI) selection is a common technique used to minimize the effects of noise while choosing the areas that contain the most physiological information.

Given the integral role of ROI selection in rPPG signal extraction, many methods have been proposed. Kwon et al. [11] found that the forehead and cheeks have stronger rPPG signals than other areas of the face. Similar results were shown in [7], which carried out a comparison of 30 ROIs based on skin thickness. Zhao et al. [30] proposed multi-scale facial ROIs to obtain independent rPPG signals and combined them with Gaussian priors to produce a higher quality signal.

Researchers have also proposed methods that perform ROI selection dynamically over time, as dynamic ROI selection is more efficient in dealing with head motions [23, 29]. Lee et al. [12] suggested a way to choose the ROI based on pulsatile strength determined from the size of the pulsatile signal amplitude. Bobbia and colleagues [2] decomposed the human face into Temporal Superpixels (TSP) and identified the most prominent signals based on the SNR. The weighted average of the individual signals from the TSPs was calculated to obtain the final rPPG signal. Tulyakov et al. [23] used image warping to construct a rectangular region below the eyes, divided the selected region into multiple smaller ROIs, and applied self-adaptive matrix completion (SAMC) to extract the optimal rPPG signal. The group of de Haan [29] considered every facial skin pixel as an independent rPPG source and proposed a framework that exploits the spatial redundancy to remove head motions artifacts from the rPPG signal.

The Dichromatic Reflectance Model (DRM) [20] is widely used in many rPPG methods to model the interactions between the light reflected from the skin and the camera. It is given by the equation:

$$L(\lambda) = m_s c_s(\lambda) + m_d c_d(\lambda) \quad (1)$$

*Joint first authors ({klwongaz,jwchin}@connect.ust.hk)

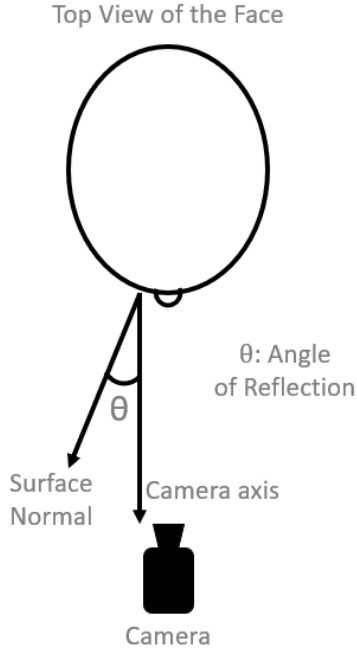


Figure 1. Illustration of the angle of reflection for a face pixel during rPPG signal extraction.

where the total detected light, L , is composed of the specular reflection (light reflected from the surface), $c_s(\lambda)$, and the diffuse reflection (light containing physiological information reflected from beneath the skin), $c_d(\lambda)$. According to the DRM, the scaling factors of the specular reflection, m_s , and diffuse reflection, m_d , strongly depend on the angle of reflection (angle between the surface normal and the camera shown in Figure 1). Despite the significance of the surface orientation for rPPG signal extraction, no studies have considered this factor for ROI selection.

In this paper, we propose a novel face angle representation—that is, an angle map—to investigate the surface orientation of the face for improved rPPG signal extraction. We conduct our investigation and analysis on a public

database, UBFC-rPPG [2], and demonstrate the feasibility of using angle maps for dynamic ROI selection. Below is the summary of our main contributions:

- It is the first study of the effect of surface orientation on rPPG signal extraction.
- It proposes a novel facial representation of the skin’s surface orientation, angle map, that is a 2-dimensional image containing the angle of reflection of each facial pixel.
- It demonstrates the potential of the angle map for dynamically selecting ROIs based on their surface angle orientation, thereby optimising the strength of the extracted rPPG signals.

2. Methods

2.1. Surface Orientation Calculation

Figure 2 shows the overall pipeline to generate an angle map from an image. For each image frame, we applied the MediaPipe FaceMesh [13] to detect 468 3D landmarks of the subject’s face. The 3D facial landmarks serve as reference points for the subsequent calculation of the surface normal vectors and angles of reflection (Figure 1) of the facial pixels.

We defined the set of possible surface normal vectors at landmark j , S_j , as:

$$S_j = \{\vec{v}_{ji} \times \vec{v}_{jk} \mid i = [1 .. m-1], k = [i+1 .. m], m \in \mathbf{Z}^+\} \quad (2)$$

where v_{ji} denotes the vector from landmark j to a neighboring landmark i , v_{jk} denotes the vector from landmark j to another neighboring landmark k , and m is a positive integer representing the number of neighboring landmarks used to estimate the set of possible surface normal vectors for landmark j . Inspired by [31], we used the analysis of covariance (ANCOVA) to choose the most representative surface normal at landmark j from the set. Finally, the angle of reflection of landmark j , θ_j , is estimated as:

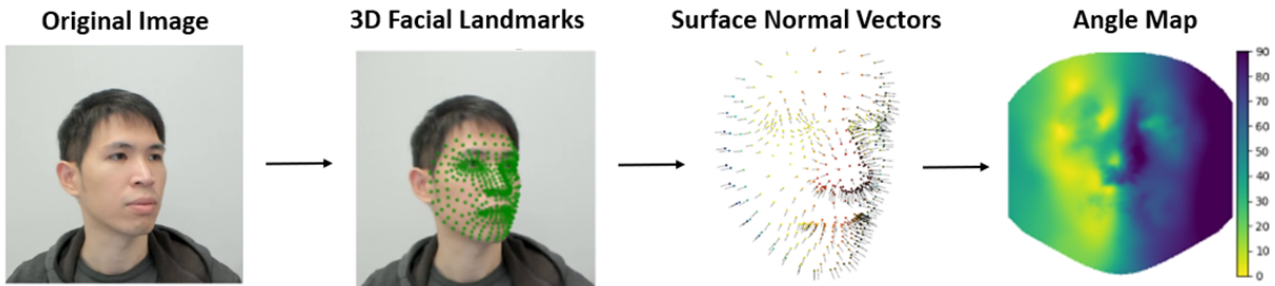


Figure 2. Process of generating an angle map.

$$\theta_j = \arccos\left(\frac{\vec{N}_j \cdot \vec{Z}}{|\vec{N}_j| |\vec{Z}|}\right) \quad (3)$$

where \vec{N}_j is the surface normal of landmark j and \vec{Z} is the unit vector of the camera axis.

2.2. Angle Map Generation

After calculation of the surface orientation, we mapped the angle of reflection of each 3D landmark to the corresponding 2D location of the landmark shown in Figure 3. We extrapolated the surrounding area of each landmark to generate the final angle map. Figure 4 shows how the angle map changes according to the subject's face orientation. Additionally, the right column illustrates the selected area when a 45° threshold is applied to the angle map. In other words, pixels with an angle of reflection larger than 45° are removed.

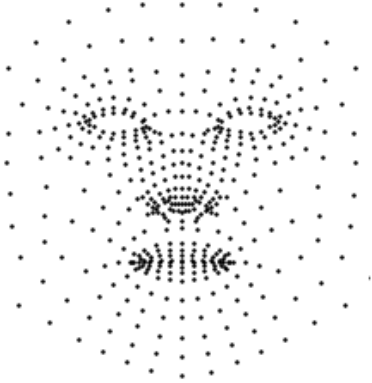


Figure 3. Corresponding 2D locations of the facial landmarks detected using [13].

2.3. Evaluation

The rPPG signals of the face are necessary for evaluating the feasibility of the angle map for dynamic ROI selection. To extract the rPPG signals, we applied skin segmentation [3] on the original frames to remove areas with low SNR. Next, we performed histogram analysis on the face images in the HSV color space and calculated the Highest Posterior Density (HPD) with $\alpha = 0.05$. By using the HPD and defining threshold values for all color channels, we masked out the non-skin areas in the video frames. Using a similar transformation as Section 2.2, we mapped the RGB values of the 3D facial landmarks to a corresponding 2D image array with the same dimensions as the angle map. Lastly, we utilized a chrominance-based method [4] to obtain the rPPG signal of every pixel within the 2D image array.

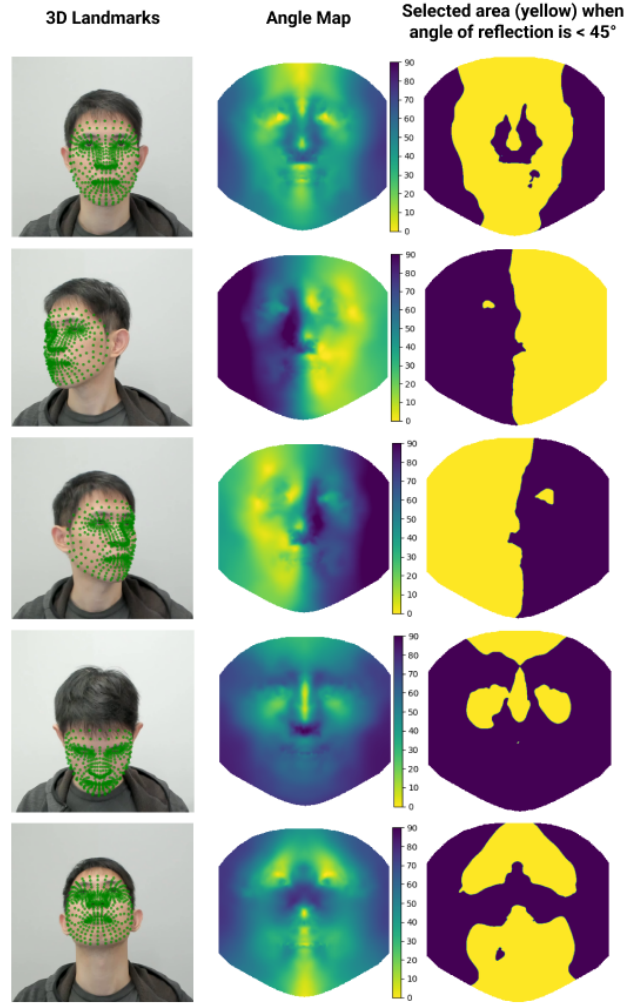


Figure 4. Example of how the angle map changes according to the face direction. Left column shows 3D face landmarks overlaid on the face images. Middle column shows the corresponding angle maps. Right column shows the selected area (yellow) when the angle of reflection is $< 45^\circ$.

The following metrics were used to evaluate the effect of surface orientation, specifically the angle of reflection, on the extracted rPPG signals:

- **Correlation Coefficient** (ρ) between the extracted rPPG signal X and the ground truth BVP Y of each facial pixel. The equation is as follows:

$$\rho = \frac{(X - \mu_X)(Y - \mu_Y)}{\sigma_X \sigma_Y} \quad (4)$$

where μ_X and μ_Y denote the mean value of X and Y , while σ_X and σ_Y denote their variance, respectively. $\rho = 1$ and $\rho = -1$ correspond, respectively, to the strongest positive and negative linear correlation be-

tween the two signals, while $\rho = 0$ indicates there is no linear correlation at all.

- **Signal-to-Noise Ratio (SNR)** of the rPPG and BVP signals. The SNR is calculated by dividing energy distribution inside the desired band by the energy in the spectrum that lies outside of the desired band. The formula by [4] was adopted:

$$SNR = 10 \log_{10} \frac{\sum_{f=30}^{240} (U_t(f) \hat{S}(f))^2}{\sum_{f=30}^{240} ((1 - U_t(f)) \hat{S}(f))^2} \quad (5)$$

where $U_t(f)$ is a binary template window defined in [4], $\hat{S}(f)$ is the spectrum of the rPPG signal, and f is the frequency in beats per minute (bpm). The desired signal band falls within the range of the general human pulse rate, i.e. 30bpm to 240bpm.

3. Experiments and Results

3.1. Dataset

The **UBFC-rPPG dataset** [2] is composed of 50 1-minute-long videos in 8-bits RGB uncompressed format. Each subject is situated 1 meter from the camera and required to play a time-sensitive mathematical game intended to increase his/her heart rate. The ground-truth heart rate and PPG data are directly available in the dataset.

3.2. Validating the Impact of Angle of Reflection on rPPG Signal Quality

We used pixel binning to average out sensor noise and produce a 16x16 array representing individual ROIs of the face (hereafter called pixel ROIs). Figure 5 illustrates the average correlation between the extracted rPPG signal and the ground truth BVP signal (left) and the average angle of reflection (right) for each pixel ROI over the 50 subjects in the UBFC-rPPG dataset. The eyes and lip areas were masked off since we only wanted to consider the skin surface. It is worth noting that the pixel ROIs near the cheeks and forehead areas have higher correlation coefficients and smaller angles of reflection.

Figure 6 illustrates the plot of the average correlation coefficient between the rPPG and BVP signals against the angle of reflection of the pixel ROIs. We observe that decreasing the angle of reflection significantly increases the correlation coefficient between the predicted and ground truth signals ($p < 0.001$).

3.3. Size of Pixel ROI Array

To further validate our hypothesis, we performed pixel binning to produce additional pixel ROI arrays of different sizes: 8x8 and 32x32. As shown in Figure 7, the inversely proportional relationship between the correlation coefficient

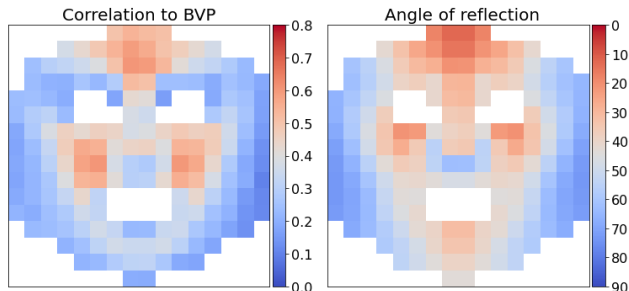


Figure 5. Average correlation coefficient between the rPPG and BVP signals for each pixel ROI (left) and average angle of reflection for each pixel ROI (right) over all subjects in the UBFC-rPPG dataset.

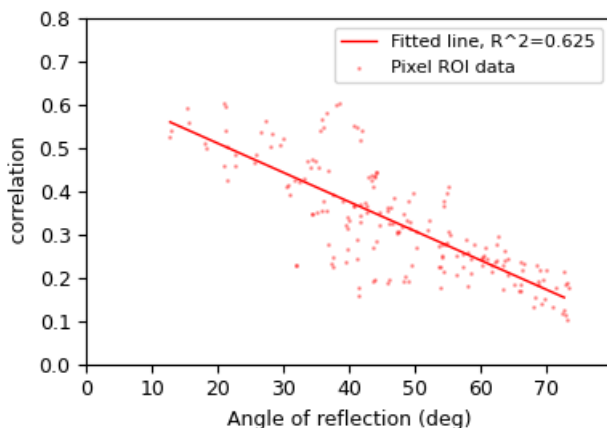


Figure 6. Average correlation coefficient between extracted rPPG signal and ground truth BVP signal versus the angle of reflection per pixel ROI.

and the angle of reflection still holds for pixel ROI arrays of different sizes. We also observe a slight decrease in the R-squared (R^2) value as the size of the pixel ROI array increases, which could be due to increased sensor noise captured by each pixel ROI in large pixel ROI arrays.

3.4. Thresholding Angle Map for ROI Selection

To investigate the feasibility of using the angle map for dynamic ROI selection, we applied different thresholds to mask off pixel ROIs based on their angle of reflection. We averaged the remaining pixel ROIs of the masked face to extract the rPPG signal for subsequent analysis. Figure 8 and 9 show the average correlation coefficient between the extracted rPPG signal and ground truth BVP and the average SNR of the extracted rPPG signals at different threshold angles, respectively. By setting a threshold at 45° (pixels ROIs with an angle of reflection above 45° are masked off), the rPPG signal extracted from the masked face, regardless of the size of the pixel ROI array, has a significantly higher cor-

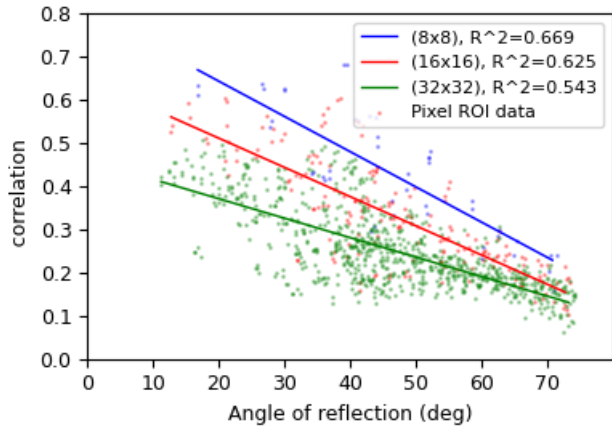


Figure 7. Average correlation coefficient between extracted rPPG signal and ground truth BVP signal versus the angle of reflection per pixel ROI for arrays of different sizes.

relation coefficient and SNR than the rPPG signal extracted from the full face benchmark ($p < 0.05$). We hypothesize that a smaller angle threshold does not achieve better signal quality due to over-masking of the pixel ROIs, thus increasing the amount of sensor noise during rPPG signal extraction.

Another benefit of applying the angle mask for ROI selection is to desensitize the influence of the size of the pixel ROI array on the quality of the rPPG signal. As shown in Figure 7, the correlation between the rPPG signal and its ground truth are affected by the size of the pixel ROI array. After applying the threshold, the influence has been reduced as illustrated in Figure 8, thereby increasing the robustness of the angle mask for rPPG signal extraction. In addition, the switching from the linear relationship in Figure 6 to the inverted U-shape curves in Figures 8 and 9 enable a data structure for optimisation of signal quality.

4. Conclusion and Future Works

We report the first study on the effects of surface orientation on rPPG by using a novel angle mask and illustrated the impact of the angle of reflection on the quality of the extracted rPPG signal. Our results show that decreasing the angle of reflection significantly and linearly increases the correlation between the extracted rPPG signal and ground truth BVP. The dependence of the extracted signals on the surface orientation explains why the ROIs around the cheek and forehead areas of front-facing subjects mostly contained stronger rPPG signals. This demonstrates the possibility of using the angle mask for dynamically selecting ROIs, thereby optimising the rPPG signal extraction process.

We will take our future works in two directions. First, the quality of the rPPG signal in different face areas can be fur-

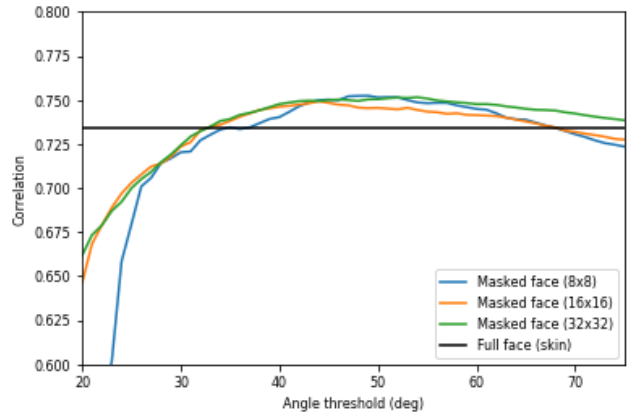


Figure 8. Average correlation between extracted rPPG signal and ground truth BVP at different threshold values.

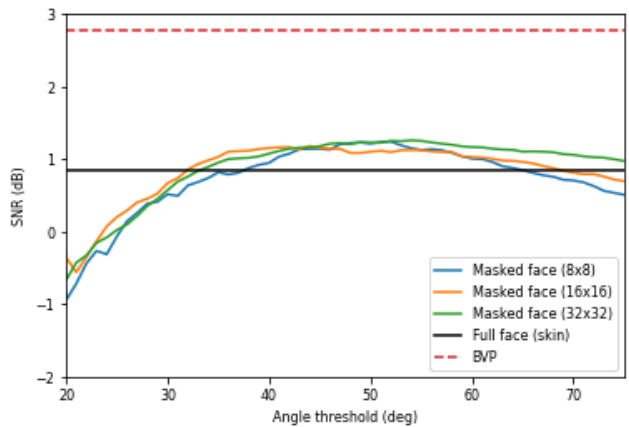


Figure 9. Average SNR of the extracted rPPG signals at different threshold values.

ther investigated with subjects facing in different directions and undergoing different types of head motions. We also want to explore the angle map for optimising remote measurement of vital signs, such as utilizing it as an attention mechanism for training neural networks. Second, we want to refine the methods for dynamically selecting ROI based on the surface orientation of other body parts and study its relationship with skin thickness. This work will enable us to utilize rPPG for accurate remote measurement of vital signs while protecting users' privacy.

References

- [1] Robert Amelard, Christian Scharfenberger, Farnoud Kazemzadeh, Kaylen J Pfisterer, Bill S Lin, David A Clausi, and Alexander Wong. Feasibility of long-distance heart rate monitoring using transmittance photoplethysmographic imaging (ppgi). *Scientific reports*, 5(1):1–11, 2015.
- [2] Serge Bobbia, Richard Macwan, Yannick Benezeth, Alamin Mansouri, and Julien Dubois. Unsupervised skin tissue seg-

- mentation for remote photoplethysmography. *Pattern Recognition Letters*, 124:82–90, 2019.
- [3] Giuseppe Boccignone, Donatello Conte, Vittorio Cuculo, Alessandro D’Amelio, Giuliano Grossi, and Raffaella Lanzarotti. An open framework for remote-PPG methods and their assessment. *IEEE Access*, pages 1–1, 2020.
 - [4] Gerard De Haan and Vincent Jeanne. Robust pulse rate from chrominance-based rppg. *IEEE Transactions on Biomedical Engineering*, 60(10):2878–2886, 2013.
 - [5] Justin R Estepp, Ethan B Blackford, and Christopher M Meier. Recovering pulse rate during motion artifact with a multi-imager array for non-contact imaging photoplethysmography. In *2014 IEEE International Conference on Systems, Man, and Cybernetics (SMC)*, pages 1462–1469. IEEE, 2014.
 - [6] In Cheol Jeong and Joseph Finkelstein. Introducing contactless blood pressure assessment using a high speed video camera. *Journal of medical systems*, 40(4):77, 2016.
 - [7] Dae-Yeol Kim, Kwangkee Lee, and Chae-Bong Sohn. Assessment of roi selection for facial video-based rppg. *Sensors*, 21(23):7923, 2021.
 - [8] LingQin Kong, YuHeng Wu, YueJin Zhao, LiQuan Dong, Mei Hui, Ming Liu, and XiaoHua Liu. Robust imaging photoplethysmography in long-distance motion. *IEEE Photonics Journal*, 12(3):1–12, 2020.
 - [9] Lingqin Kong, Yuejin Zhao, Liqun Dong, Yiyun Jian, Xiaoli Jin, Bing Li, Yun Feng, Ming Liu, Xiaohua Liu, and Hong Wu. Non-contact detection of oxygen saturation based on visible light imaging device using ambient light. *Optics express*, 21(15):17464–17471, 2013.
 - [10] Mayank Kumar, Ashok Veeraraghavan, and Ashutosh Sabharwal. Distanceppg: Robust non-contact vital signs monitoring using a camera. *Biomedical optics express*, 6(5):1565–1588, 2015.
 - [11] Sungjun Kwon, Jeehoon Kim, Dongseok Lee, and Kwang-suk Park. Roi analysis for remote photoplethysmography on facial video. In *2015 37th Annual International Conference of the IEEE Engineering in Medicine and Biology Society (EMBC)*, pages 4938–4941. IEEE, 2015.
 - [12] Keonsoo Lee and Yunyoung Nam. Optimal roi determination for obtaining ppg signals from a camera on a smartphone. *Journal of Electrical Engineering and Technology*, 13(3):1371–1376, 2018.
 - [13] Camillo Lugaresi, Jiuqiang Tang, Hadon Nash, Chris McClanahan, Esha Uboweja, Michael Hays, Fan Zhang, Chuoling Chang, Ming Guang Yong, Juhyun Lee, et al. Mediapipe: A framework for building perception pipelines. *arXiv preprint arXiv:1906.08172*, 2019.
 - [14] Carlo Massaroni, Daniel Simões Lopes, Daniela Lo Presti, Emiliano Schena, and Sergio Silvestri. Contactless monitoring of breathing patterns and respiratory rate at the pit of the neck: A single camera approach. *Journal of Sensors*, 2018, 2018.
 - [15] Yuriy Mironenko, Konstantin Kalinin, Mikhail Kopeliovich, and Mikhail Petruschan. Remote photoplethysmography: Rarely considered factors. In *Proceedings of the IEEE/CVF Conference on Computer Vision and Pattern Recognition (CVPR) Workshops*, June 2020.
 - [16] Andreia V Moço, Sander Stuijk, and Gerard de Haan. New insights into the origin of remote ppg signals in visible light and infrared. *Scientific reports*, 8(1):1–15, 2018.
 - [17] Ewa M Nowara, Tim K Marks, Hassan Mansour, and Ashok Veeraraghavan. Near-infrared imaging photoplethysmography during driving. *IEEE Transactions on Intelligent Transportation Systems*, 2020.
 - [18] Ewa M Nowara, Daniel McDuff, and Ashok Veeraraghavan. A meta-analysis of the impact of skin tone and gender on non-contact photoplethysmography measurements. In *Proceedings of the IEEE/CVF Conference on Computer Vision and Pattern Recognition Workshops*, pages 284–285, 2020.
 - [19] Ming-Zher Poh, Daniel J McDuff, and Rosalind W Picard. Advancements in noncontact, multiparameter physiological measurements using a webcam. *IEEE transactions on biomedical engineering*, 58(1):7–11, 2010.
 - [20] Steven A Shafer. Using color to separate reflection components. *Color Research & Application*, 10(4):210–218, 1985.
 - [21] Toshiyo Tamura. Current progress of photoplethysmography and spo2 for health monitoring. *Biomedical engineering letters*, 9(1):21–36, 2019.
 - [22] Akito Tohma, Maho Nishikawa, Takuya Hashimoto, Yoichi Yamazaki, and Guanghao Sun. Evaluation of remote photoplethysmography measurement conditions toward telemedicine applications. *Sensors*, 21(24):8357, 2021.
 - [23] Sergey Tulyakov, Xavier Alameda-Pineda, Elisa Ricci, Lijun Yin, Jeffrey F Cohn, and Nicu Sebe. Self-adaptive matrix completion for heart rate estimation from face videos under realistic conditions. In *Proceedings of the IEEE conference on computer vision and pattern recognition*, pages 2396–2404, 2016.
 - [24] Mark van Gastel, Sander Stuijk, and Gerard de Haan. Motion robust remote-ppg in infrared. *IEEE Transactions on Biomedical Engineering*, 62(5):1425–1433, 2015.
 - [25] Wim Verkrusse, Lars O Svaasand, and J Stuart Nelson. Remote plethysmographic imaging using ambient light. *Optics express*, 16(26):21434–21445, 2008.
 - [26] Dingliang Wang, Xuezhi Yang, Xuenan Liu, Likun Ma, Longwei Li, and Wenjin Wang. Photoplethysmography-based blood pressure estimation combining filter-wrapper collaborated feature selection with lasso-lstm model. *IEEE Transactions on Instrumentation and Measurement*, 70:1–14, 2021.
 - [27] Wenjin Wang and Albertus C den Brinker. Camera-based respiration monitoring: Motion and ppg-based measurement. In *Contactless Vital Signs Monitoring*, pages 79–97. Elsevier, 2022.
 - [28] Wenjin Wang and Caifeng Shan. Impact of makeup on remote-ppg monitoring. *Biomedical Physics & Engineering Express*, 6(3):035004, 2020.
 - [29] Wenjin Wang, Sander Stuijk, and Gerard De Haan. Exploiting spatial redundancy of image sensor for motion robust rppg. *IEEE transactions on Biomedical Engineering*, 62(2):415–425, 2014.
 - [30] Changchen Zhao, Weiran Han, Zan Chen, Yongqiang Li, and Yuanjing Feng. Remote estimation of heart rate based on

multi-scale facial rois. In *Proceedings of the IEEE/CVF Conference on Computer Vision and Pattern Recognition Workshops*, pages 278–279, 2020.

- [31] Qian-Yi Zhou, Jaesik Park, and Vladlen Koltun. Open3D: A modern library for 3D data processing. *arXiv:1801.09847*, 2018.